Available online at www.sciencedirect.com
SCIENCE DIRECT®

Journal of the European Ceramic Society 23 (2003) 1313–1328
www.elsevier.com/locate/jeurceramsoc

Influence of electric fields on the fracture of ferroelectric ceramics

Andreas Ricoeur*, Meinhard Kuna

Freiberg University of Mining and Technology, Insitute of Mechanics and Fluid Dynamics, Lampadiusstr. 4, 09596 Freiberg, Germany

Received 1 March 2002; received in revised form 25 August 2002; accepted 7 September 2002

Abstract

This paper deals with the fracture mechanics of piezoelectric solids. All investigations consider a single crack, which is exposed to combined electrical and mechanical loading. The main subject of interest is the influence of electric fields on the fracture toughness of ferroelectric ceramics and the derivation of an appropriate fracture criterion. Numerical techniques are presented, allowing for the calculation of fracture quantities, i.e. stress intensity factors and energy release rates, once the piezoelectric field problem has been solved for arbitrary crack configurations using the finite element method. In order to describe a possible shielding of the crack tip due to ferroelectric/elastic domain switching events, a micromechanical model has been developed, based on a closed form solution of the piezoelectric field problem. In order to verify the theory, fracture experiments on barium titanate DCB specimens have been evaluated and compared to predictions of the model.

Keywords: $BaTiO_3$; Ferroelectric domains; Ferroelectric properties; Finite element methods; Fracture toughness; Piezoelectric properties; Switch-toughening

1. Introduction

When problems of optimum performance and material processing are solved, the sucess of smart structures with integrated functional ceramics essentially depends on their strength and reliability. Because of the intrinsic brittleness of piezoelectric ceramics, cracks play an important role by drastically reducing the fracture strength and fatigue limits. Since all non-elastic processes are restricted to regions around the crack tip, which are small compared to relevant crack lengths, the concepts of linear elastic fracture mechanics[1,2] (LEFM) are applied in our investigations. The state of the art in linear piezoelectric fracture mechanics has recently been compiled by Zhang et al.[3] and by Qin.[4]

In general, the smart ceramics are exposed to both mechanical and electrical loads causing stresses and electric displacements in the body. At crack tips these fields show a $1/\sqrt{r}$ singularity,[5,6] where r denotes the distance from the crack tip, see Fig. 1. The local asymptotic distributions of stresses σ_{ij} and electric displacements D_i are qualitatively identical at all crack tips. Following the classical K-concept, the crack tip fields can be expressed in terms of stress intensity factors K_{I}, K_{II} and K_{III}, corresponding to the three mechanical crack opening modes, and an electric intensity factor K_{IV}:

$$\lim_{r\to 0}\sigma_{ij}(r,\theta) = \frac{1}{\sqrt{2\pi r}}\left[K_{\mathrm{I}} f_{ij}^{\mathrm{I}}(\theta)+K_{\mathrm{II}} f_{ij}^{\mathrm{II}}(\theta)+K_{\mathrm{III}} f_{ij}^{\mathrm{III}}(\theta)+K_{\mathrm{IV}} f_{ij}^{\mathrm{IV}}(\theta)\right]$$

$$\lim_{r\to 0} D_i(r,\theta) = \frac{1}{\sqrt{2\pi r}}\left[K_{\mathrm{I}} g_i^{\mathrm{I}}(\theta)+K_{\mathrm{II}} g_i^{\mathrm{II}}(\theta)+K_{\mathrm{III}} g_i^{\mathrm{III}}(\theta)+K_{\mathrm{IV}} g_i^{\mathrm{IV}}(\theta)\right] \quad (1)$$

In Eq. (1) θ is the polar angle around the crack tip, $f_{ij}(\theta)$ and $g_i(\theta)$ are angular functions characterising the asymptotic near field distribution. They depend on the orientation of the crack in the anisotropic material and on the crack opening modes. Besides the four intensity factors, the loading of the crack tip can be described by an energy release rate G. It is defined as the change of

* Corresponding author. Tel.: +49-37-12-390; fax: +49-37-312-21-95.
E-mail address: andreas.ricoeur@imfd.tu-freiberg.de (A. Ricoeur).

0955-2219/03/$ - see front matter © 2002 Elsevier Science Ltd. All rights reserved.
PII: S0955-2219(02)00302-3

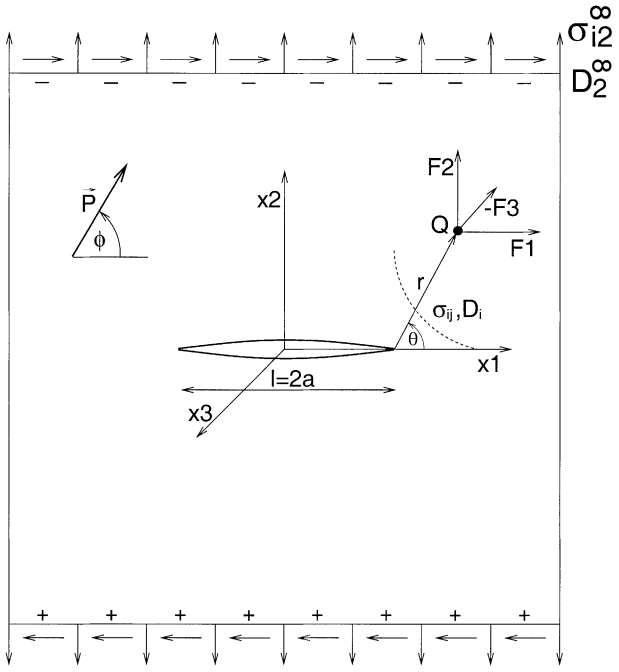

Fig. 1. Griffith crack with remote loads σ_{i2}^{∞}, D_2^{∞} and point loads F_1, F_2, F_3 and Q.

the total energy Π of the cracked body related to an incremental growth of the crack area ΔA:

$$G = -\lim_{\Delta A \to 0}\left(\frac{\Delta \Pi}{\Delta A}\right) = -\frac{\mathrm{d}\Pi}{\mathrm{d}A} \tag{2}$$

The energy release rate and the intensity factors can be related by the equation[5]

$$G = \frac{1}{2}(K_{\mathrm{II}}, K_{\mathrm{I}}, K_{\mathrm{III}}, K_{\mathrm{IV}})\mathbf{Y}(\boldsymbol{C}, \boldsymbol{e}, \boldsymbol{\kappa})\begin{pmatrix} K_{\mathrm{II}} \\ K_{\mathrm{I}} \\ K_{\mathrm{III}} \\ K_{\mathrm{IV}} \end{pmatrix} \tag{3}$$

with a generalised Irwin matrix $\mathbf{Y}$, which is a function of elastic, piezoelectric and dielectric material tensors $\boldsymbol{C}$, $\boldsymbol{e}$ and $\boldsymbol{\kappa}$ as well as the orientation of the crack with respect to the material axes.

In order to evaluate the strength of a cracked structure, relevant fracture quantities have to be related to a critical, material inherent value. Generally, a fracture criterion can be formulated by an equation of the kind

$$B(K_{\mathrm{I}}, \ldots, K_{\mathrm{IV}}) = B_C(\Delta a, K_{\mathrm{I}}, \ldots, K_{\mathrm{IV}}) \tag{4}$$

In Eq. (4), the fracture quantity B represents the applied loading side, which can be expressed in terms of the intensity factors. In the single mode case, the corresponding stress intensity factor or the energy release rate are chosen for B. In mixed mode fracture mechanics, the fracture criterion is more complicated and in the case of electromechanical loading still unknown. The critical value B_C on the right hand side of Eq. (4) is material dependent, although not necessarily constant. In this connection microstructural effects within the fracture process zone may play an important role.[7,8] The process zone is a small region around the crack tip, where all irreversible processes going along with fracture take place. In ferroelectrics the fracture process zone is dominated by domain switching.[9,10] These microstructural effects may, for example, cause a dependence of B_C on the crack growth Δa (R–curve effect). Moreover, the material resistance may depend on the crack tip fields σ_{ij} and D_i, controlling the microstructural effects within the process zone. According to Eq. (1) the crack tip fields are uniquely determined by the intensity factors $K_{\mathrm{I}}, \ldots, K_{\mathrm{IV}}$.

In this paper, we first present an analytical solution of the coupled piezoelectric field problem of a cracked body, yielding all crack tip fields, fracture quantities and crack weight functions, respectively. Afterwards, numerical methods, which have been developed for the calculation of field intensity factors and energy release rates are presented. They can be applied to the fracture mechanics analysis of arbitrary cracks in piezoelectric structures as well as to the evaluation of electromechanical fracture experiments. As an example, experiments with double cantilever beams (DCB) made of poled barium titanate are presented and analysed. Driven by a wedge, a mechanically loaded crack is propagated stably for several millimeters. During crack growth, an electric field is switched on and off, to investigate the influence of electric loads on the fracture quantities. To understand the observed effects, a micromechanical model of the fracture process zone, based on the analytical framework is developed. The influence of small scale ferroelectric/elastic domain switching on the fracture toughness is investigated giving insight into the right hand side of the fracture criterion, Eq. (4). The results are compared to experimental findings.

2. Analytical framework of piezoelectric fracture

2.1. Closed form solution of the piezoelectric Griffith crack problem

The subject under consideration is a through-thickness crack with a length $2a$ in an infinitely wide piezoelectric plate exposed to remote stresses and electric displacements, see Fig. 1. The point loads F_1, F_2, F_3 and Q are disregarded for the moment. The Stroh formalism is applied to solve the anisotropic, electromechanical field problem, yielding stresses σ_{ij}, electric displacements D_i, mechanical displacements u_i and the electric potential ϕ within the cracked body, see.[11]

The strain tensor ε_{ij} and the electric field vector E_i can be introduced as:

$$\varepsilon_{ij} = \frac{1}{2}\left(u_{i,j} + u_{j,i}\right)$$
$$E_i = -\phi,_i \tag{5}$$

The governing equations are those of linear elastostatics and electrostatics:[5,6]

$$\sigma_{ij,j} + b_i = 0$$
$$D_{i,i} - \omega_V = 0 \tag{6}$$

Volume loads b_i and volume charges ω_V will be neglected in the following. The constitutive behavior of piezoelectric materials is described by

$$\sigma_{ij} = C_{ijkl}u_{k,l} + e_{ijl}\phi,_l$$
$$D_i = e_{ikl}u_{k,l} - \kappa_{il}\phi,_l \tag{7}$$

with the elastic, piezoelectric and dielectric material tensors C_{ijkl}, e_{ijl} and κ_{il}, respectively. Inserting Eq. (7) into Eq. (6) yields a set of partial differential equations describing a general piezoelectric field problem in terms of displacements and potentials. To solve these equations the displacements and the electric potential are represented by the function

$$u_N = \begin{pmatrix} u_i \\ \phi \end{pmatrix} = \begin{pmatrix} A_i \\ A_4 \end{pmatrix} f(z) = A_N f(z); \quad z = x_1 + p x_2 \tag{8}$$

Here, the mechanical displacements and the electric potential are collected in the matrix u_N. It will be agreed that indices in capital letters comprise the four fracture modes {II, I, III, IV}, thus running over {1, 2, 3, 4}. The variable z allows u_i and ϕ to depend on the coordinates x_1 and x_2. Since derivatives with respect to x_3 disappear, the strain ε_{33} and the electric field intensity E_3 are zero [Eq. (5)]. Applying Eq. (8) yields a generalised eigenvalue problem with eigenvalues p and eigenvectors A_N. The characteristic equation is a polynomial of 8th degree, which requires numerical solution. Since the coefficients of the characteristic polynomial, being functions of material constants, are real, the roots yield four conjugate complex pairs of eigenvalues. The corresponding conjugate complex pairs of eigenvectors A_N are linear independent in most cases of interest.

In order to obtain a solution in terms of stresses and electric displacements, Eq. (8) is inserted into the constitutive equations, Eq. (7). To calculate the fields in a cracked body, the function $f(z)$ in Eq. (8) has to be specified in terms of boundary conditions, see Fig. 1. Across the ligament ($x_2 = 0$, $|x_1| > a$) all fields are supposed to be continuous. On the crack faces ($x_2 = 0$, $|x_1| < a$) stresses and electric displacements are denoted by σ_{i2}^S and the surface charge density D_2^S. Considering these boundary conditions, the function $f(z)$ is determined applying the Fourier transformation yielding two sets of dual integral equations, which are solved following Pohanka and Smith.[12] The results for stresses and electric displacements are[13]

$$\begin{pmatrix} \sigma_{i1} \\ D_1 \end{pmatrix} = -\Re\left\{ M_{M\alpha} N_{\alpha N} p_\alpha \left[\left(z_\alpha^2 - \alpha^2\right)^{-\frac{1}{2}} z_\alpha - 1 \right] \right\} T_N$$
$$\begin{pmatrix} \sigma_{i2} \\ D_2 \end{pmatrix} = \Re\left\{ M_{M\alpha} N_{\alpha N} \left[\left(z_\alpha^2 - a^2\right)^{-\frac{1}{2}} z_\alpha - 1 \right] \right\} T_N \tag{9}$$

where $\Re\{\ldots\}$ denotes the real part. The index α is introduced to take into account the summation over the number q of linear independent eigenvectors ($q \leqslant 4$). The matrix $M_{M\alpha}$ only depending on material properties is defined:

$$M_{M\alpha} = \begin{pmatrix} (C_{i2k1} + C_{i2k2}p_\alpha)A_{k\alpha} + (e_{i12} + e_{i22}p_\alpha)A_{4\alpha} \\ (e_{2k1} + e_{2k2}p_\alpha)A_{k\alpha} - (\kappa_{21} + \kappa_{22}p_\alpha)A_{4\alpha} \end{pmatrix} \tag{10}$$

and $N_{\alpha N}$ is the inverse of $M_{M\alpha}$. The vector $\mathrm{T_N} = \left(\sigma_{i2}^S, D_2^S\right)^T$ expresses the fields on the crack faces.

Displacements and the electric potential are derived from Eq. (8):

$$\begin{pmatrix} u_i \\ \phi \end{pmatrix} = \Re\left\{ A_{M\alpha} N_{\alpha N} \left[\left(z_\alpha^2 - \alpha^2\right)^{\frac{1}{2}} - z_\alpha \right] \right\} T_N \tag{11}$$

Eqs. (9) and (11) provide the complete mechanical and electrical field distributions around a crack due to loads acting on the crack faces. Moreover, it can be applied to the solution of the boundary value problem shown in Fig. 1 with remote loads σ_{i2}^∞ and D_2^∞. Furthermore, different crack boundary conditions, i.e. the influence of electric fields within the opened crack can be taken into account. The equilibrium of charge densities $\omega = -D_i n_i$ and stresses $t_i = \sigma_{ij} n_j$ on the crack faces ($n_1 = n_3 = 0$) requires

$$\sigma_{i2}^S = \sigma_{i2}^\infty - \sigma_{i2}^C$$
$$D_2^S = D_2^\infty - D_2^C \tag{12}$$

σ_{i2}^C and D_2^c denote fields within the crack at the interface to the piezoelectric material. Free surface charges and tractions on the crack faces have been neglected. Following the superposition principle, in Eq. (12) the remote loads have been expressed by equivalent loads on the crack faces, which are identical with σ_{i2}^∞ and D_2^∞ in this simple case. The medium within the crack is supposed not to have any elastic properties, therefore σ_{i2}^C will be neglected in the following. The charge density D_2^C takes into account the finite electric permeability of the crack. Neglecting D_2^C makes the crack impermeable with respect to electric fields.

Introducing polar coordinates r, θ (see Fig. 1), the asymptotic fields around the crack tip can be derived from Eqs. (9) and (11) for $r \to 0$:

$$\begin{pmatrix} \sigma_{i1} \\ D_1 \end{pmatrix} = -\sqrt{\frac{a}{2r}}\Re\left\{ M_{M\alpha}N_{\alpha N}\frac{p_\alpha}{\sqrt{\cos\theta + p_\alpha \sin\theta}} \right\} T_N$$

$$\begin{pmatrix} \sigma_{i2} \\ D_2 \end{pmatrix} = \sqrt{\frac{a}{2r}}\Re\left\{ M_{M\alpha}N_{\alpha N}\frac{1}{\sqrt{\cos\theta + p_\alpha \sin\theta}} \right\} T_N$$

$$\begin{pmatrix} u_i \\ \phi \end{pmatrix} = \sqrt{2ar}\Re\left\{ A_{M\alpha}N_{\alpha N}\sqrt{\cos\theta + p_\alpha \sin\theta} \right\} T_N \qquad (13)$$

2.2. Calculation of field intensity factors and the energy release rate

The field intensity factors K_{I}, K_{II}, K_{III} and K_{IV} for a Griffith crack in a piezoelectric material under electromechanical loads can be derived from the near tip solutions, Eq. (13). Comparing Eqs. (1) and (13) yields

$$K_N = \begin{pmatrix} K_{\mathrm{II}} \\ K_{\mathrm{I}} \\ K_{\mathrm{III}} \\ K_{\mathrm{IV}} \end{pmatrix} = \sqrt{\pi a}\begin{pmatrix} \sigma_{12}^{\infty} \\ \sigma_{22}^{\infty} \\ \sigma_{32}^{\infty} \\ D_2^{\infty} - D_2^{C} \end{pmatrix} = \sqrt{\pi a}\, T_N \qquad (14)$$

whereby the angular functions $f_{ij}^{L}(\theta)$ (superscript $L \equiv \{\mathrm{II}, \mathrm{I}, \mathrm{III}, \mathrm{IV}\}$) correspond to the $\Re\{\ldots\}$ terms in Eq. (13). The energy release rate G is calculated applying the crack closure integral.[3,4,6] A crack is considered which has grown by the amount Δa, see Fig. 2. A polar coordinate system (r, θ) is introduced with its origin at the tip of the original crack a. The specific work, which is necessary to close the crack at the location $(r = s, \theta = 0)$ is approximately

$$\frac{\mathrm{d}W}{\mathrm{d}s} \approx \frac{1}{2}\sigma_{2i}(s,0)\Delta u_i(\Delta a - s, \pi) + \frac{1}{2}D_2(s,0)\Delta\phi(\Delta a - s, \pi) \qquad (15)$$

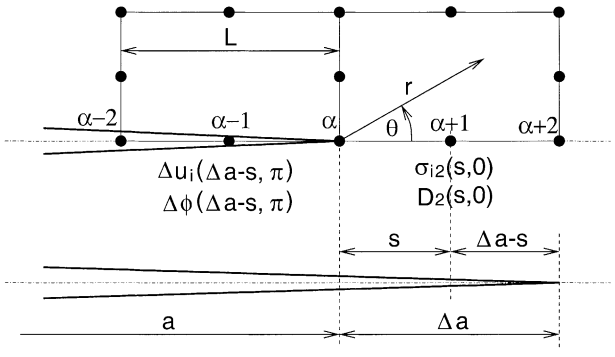

Fig. 2. Illustration of crack growth for the derivation of the crack closure integral.

with $\Delta u_i = u_i^{+} - u_i^{-}$ and $\Delta\phi = \phi^{+} - \phi^{-}$ as the difference of the displacements and the electric potential on the positive and negative crack faces. The stresses σ_{2i} and the electric displacements D_2 are those on the ligament before the crack growth. To be exact, the displacements and the potential would have to be taken from the grown crack at $(s, 0)$. Nevertheless, if Δa is small with respect to the total crack length a, all field variables may approximately be calculated for the original crack length a. In this case displacements and potentials have to be taken at $r = \Delta a - s$. Since the total crack closure work ΔW along Δa equals $-\Delta\Pi$, the energy release rate can be calculated from Eqs. (2) and (15):

$$G = \lim_{\Delta a \to 0}\frac{1}{2\Delta a}\int_0^{\Delta a}[\sigma_{2i}(s,0)\Delta u_i(\Delta a - s, \pi) + D_2(s,0)\Delta\phi(\Delta a - s, \pi)]ds \qquad (16)$$

The jumps of the displacements Δu_i and the electric potential $\Delta\phi$ over the crack faces as well as the stresses σ_{2i} and electric displacements D_2 are determined from Eq. (13). Thus, the energy release rate gives

$$G = -aT_M\Im\{A_{M\alpha}N_{\alpha N}\}T_N\lim_{\Delta a \to 0}\frac{1}{a}\int_0^{\Delta a}\sqrt{\frac{\Delta a - s}{s}}ds = = -\frac{\pi a}{2}\begin{pmatrix} \sigma_{i2}^{\infty} \\ D_2^{\infty} - D_2^{C} \end{pmatrix}\Im\{A_{M\alpha}N_{\alpha N}\}\begin{pmatrix} \sigma_{i2}^{\infty} \\ D_2^{\infty} - D_2^{C} \end{pmatrix} \qquad (17)$$

where $\Im\{\ldots\}$ means the imaginary part. In Eq. (3) the Irwin matrix has been introduced, relating intensity factors and the energy release rate. Taking into account Eqs. (14) and (17), the Irwin matrix is found to be

$$Y_{MN} = -\Im\{A_{M\alpha}N_{\alpha N}\} \qquad (18)$$

For a piezoelectric material, being transversly isotropic with the poling direction parallel or perpendicular to the crack faces, the Irwin martix can be expressed by three independent elastic constants c_T, c_L and c_A as well as one piezoelectric e and one dielectric constant κ (see Appendix B).

2.3. Piezoelectric weight functions

The derivation of anisotropic weight functions

$$h_{LN} = \frac{-1}{2\sqrt{\pi a}}\,Y_{LM}^{-1}\Re\left\{ A_{M\alpha}N_{\alpha N}\sqrt{\frac{z_\alpha + a}{z_\alpha - a}} \right\} \qquad (19)$$

for piezoelectric materials can be followed in Appendix A. By means of Eq. (19) the field intensity factors due to point forces and charges (see Fig. 1) at any location x_i can be calculated for a Griffith crack in an anisotropic, piezoelectric material:

$$K_L = \begin{pmatrix} K_{\mathrm{II}} \\ K_{\mathrm{I}} \\ K_{\mathrm{III}} \\ K_{\mathrm{IV}} \end{pmatrix} = h_{LN}(x_i)F_N = h_{LN}(x_i)\begin{pmatrix} F_1 \\ F_2 \\ F_3 \\ Q \end{pmatrix} \tag{20}$$

According to the linear superposition principle, arbitrary load configurations can be transformed into equivalent loads on the crack faces. Therefore Eq. (19) can also be used to calculate field intensity factors due to arbitrary loads considering point loads on the crack faces, where $z_\alpha = x_1$. Because of $x_1 - a < 0$ the weight functions $\overline{h}_{LN}$ for the crack faces are

$$\begin{aligned}\overline{h}_{LN} &= \pm\frac{-1}{2\sqrt{\pi a}}\, Y^{-1}_{LM}\sqrt{\frac{a+x_1}{a-x_1}}\Re\{-iA_{M\alpha}N_{\alpha N}\} \\ &= \pm\frac{1}{2\sqrt{\pi a}}\sqrt{\frac{a+x_1}{a-x_1}}\delta_{LN}\end{aligned} \tag{21}$$

The Irwin matrix has been eliminated using Eq. (18). δ_{LN} is the $L\times N$ unit tensor. Across the crack faces, the weight functions change their sign. The field intensity factors are calculated according to Eq. (20), inserting $\overline{h}_{LN}$ from Eq. (21) and adding the contributions from both crack faces. Distributed loads are taken into account by integrating along x_1 between the two crack tips:

$$K_L = \frac{1}{2\sqrt{\pi a}}\delta_{LN}\int_{-a}^{a}\left(T_N^{+}(x_1) - T_N^{-}(x_1)\right)\sqrt{\frac{a+x_1}{a-x_1}}\mathrm{d}x_1 \tag{22}$$

Considering the special case of uniform loads $T_N = \left(\sigma_{i2}^{\infty}, D_2^{\infty}\right)^T \neq f(x_1)$ at infinity, see Fig. 1, the intensity factors calculated from Eq. (22) coincide with those from Eq. (14). In Eq. (22) finite electrical permeability of the crack can be taken into account including a surface charge density D_2^C according to Eq. (12). In contrast to Eq. (14), these charges may be a function of x_1, allowing for a more accurate modelling of crack permeability.

For the investigation of the fracture process zone, crack tip weight functions will be of interest. Therefore, Eq. (19) is transformed into the polar coordinate system (r, θ), see Fig. 1. For small radii r, the crack tip weight functions are

$$h_{LN} = \frac{-1}{\sqrt{2\pi r}}\, Y^{-1}_{LM}\Re\left\{A_{M\alpha}N_{\alpha N}\frac{1}{\sqrt{\cos\theta + p_a\sin\theta}}\right\} \tag{23}$$

Fig. 3 shows the four intensity factors due to a unit point force at ($r = 10^{-3}$ m, θ), which have been calculated using the weight functions according to Eq. (23). Both load vector and material polarisation are orientated perpendicular to the crack faces pointing to the positive x_2-direction. The material data are those of barium titanate (see Appendix B). The dotted graph represents K_{I} for an isotropic elastic body with $\nu = 0.315$ and

$$h_i^{\mathrm{I}} = \frac{1}{2\sqrt{2\pi r}(1-\upsilon)} \times \begin{pmatrix} \cos\left(\frac{\theta}{2}\right)\left(2\upsilon - 1 + \sin\left(\frac{\theta}{2}\right)\sin\left(\frac{3\theta}{2}\right)\right) \\ \sin\left(\frac{\theta}{2}\right)\left(2 - 2\upsilon - \cos\left(\frac{\theta}{2}\right)\cos\left(\frac{3\theta}{2}\right)\right) \end{pmatrix} \tag{24}$$

as the isotropic weight function for the Mode-I case. Eq. (24) is derived from a more general formulation by Erdogan.[14] If the load is on the ligament ($\theta = 0$), K_{I} and K_{IV} vanish, whereas K_{II} is finite. Due to the plane strain conditions, K_{III} is zero for all angles θ. If the load is on the crack faces ($\theta = \pm\pi$) only K_{I} is finite. On the positive crack face ($\theta = +\pi$), the positive force effects a crack opening, on the negative crack face ($\theta = -\pi$) a crack closure is observed. Comparing K_{I} for the isotropic and the piezoelectric cases, the results show little difference for the chosen material constants.

3. Numerical calculation of fracture quantities

In the following, three methods are presented, allowing for the calculation of field intensity factors and the

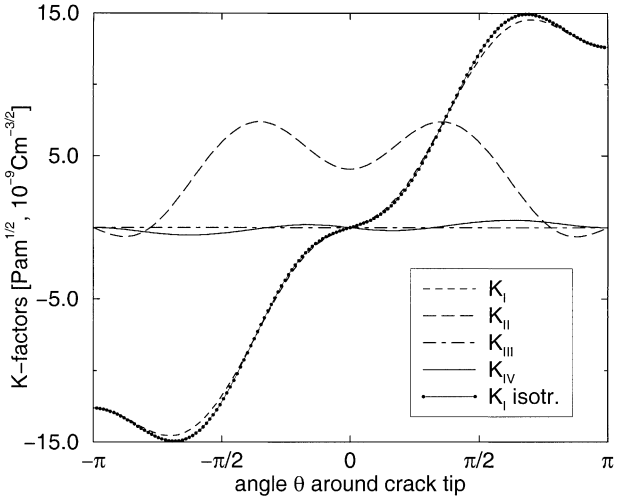

Fig. 3. Field intensity factors due to a unit point load at ($r = 10^{-3}$ m, θ). Load and polarisation perpendicular to the crack faces.

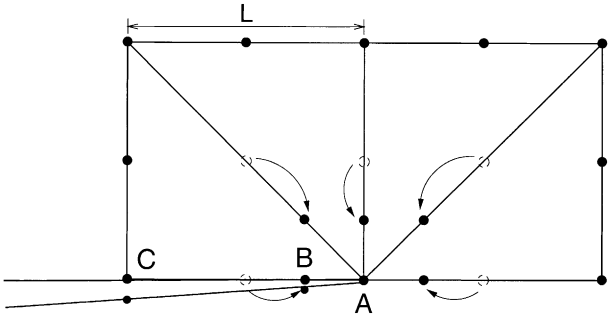

Fig. 4. Singular crack tip elements with nodes shifted in the 1/4 position.

energy release rate. All methods can be implemented as post processors based on output data of a finite element calculation of the electromechanical boundary value problem. The results obtained from the different methods have been compared[15,16] and their accuracy proved.

3.1. Singular crack tip elements (CTE method)

The stress intensity factors can be calculated using the asymptotic solutions for the crack tip displacements u_i and the electric potential ϕ. It is convenient to consider the discontinuity of the fields across the crack faces

$$\lim_{r\to 0}\Delta u_M = \lim_{r\to 0}\begin{pmatrix}\Delta u_i\\ \Delta\phi\end{pmatrix} = \sqrt{r}\sqrt{\frac{8}{\pi}}Y_{MN}K_N \tag{25}$$

where $\Delta u_M = u_M^+ - u_M^-$ denotes the difference of the field variables on the positive and negative crack faces and the matrix K_N, according to Eq. (14), contains all four intensity factors. In Eq. (25), the analytical solutions on the crack faces, see Eq. (13), are represented in terms of the Irwin matrix, see Eq. (18).

The intensity factors K_N will be determined from Eq. (25) inserting displacements u_i and electric potentials ϕ from the numerical solution of the specific boundary value problem. Therefore, special crack tip finite elements are introduced, accounting for the $\sqrt{r}$–behaviour by construction. This kind of elements has been suggested first by Barsoum[17] for the pure mechanical case. Fig. 4 shows the discretisation of the positive crack face and a part of the ligament with four triangular elements arranged arround the crack tip, which lies at node A. For the sake of simplicity, a 2D grid was chosen in Fig. 4. These special triangular elements are constructed by collapsing one edge of a regular 8-node rectangular element and shifting two mid-edge nodes to the 1/4-position, as depicted in Fig. 4. On the negative crack face the crack tip region is meshed the same way, whereas the rest of the finite element model is discretisised with regular 8-node rectangular elements. In the 3D case, the finite element mesh around the crack front consists of singular pentahedron elements and regular hexahedron elements.

With the specific shape functions of the quarter point elements[18] the discontinuity of the fields across the crack faces can be expressed for $r \to 0$:

$$\Delta u_M = \sqrt{\frac{r}{L}}\left\{4\Delta u_M(B) - \Delta u_M(C)\right\} \tag{26}$$

with the element length L and u_M at nodes B and C, see Fig. 4. Inserting Eq. (26) into Eq. (25) finally yields the field intensity factors:

$$K_M = \sqrt{\frac{\pi}{8L}}Y_{MN}^{-1}\left\{4\Delta u_N(B) - \Delta u_N(C)\right\} \tag{27}$$

For 2D calculations Eq. (27) is applied with $\Delta u_3 = 0$, yielding K_I, K_II and K_IV. For 3D calculations the crack front is meshed with a tube of pentahedron elements. In this case Eq. (27) is applied locally along the crack front.

3.2. The modified crack closure integral (MCCI method)

The calculation of the energy release rate G by the crack closure integral has been presented in Eq. (16). The numerical determination of G applying the MCCI technique has first been realised by Buchholz[19] for the pure mechanical case. The electromechanical generalisation has been investigated by different authors.[18,20,21] For the numerical realisation of Eq. (16), stresses and electric displacements are replaced by nodal forces F_i and charges ω, respectively. Instead of the integration, a summation over the nodes within Δa is performed, accounting for displacements and electric potentials at the corresponding nodes on the crack faces. A good performance was found[18] setting Δa equal to an element length L. For 8-node rectangular elements two node sets have to be taken into account, see Fig. 2:

$$G = \frac{1}{2L}\left(F_i^\alpha \Delta u_i^{\alpha-2} - \omega^\alpha \Delta\phi^{\alpha-2} + F_i^{\alpha+1}\Delta u_i^{\alpha-1} - \omega^{\alpha+1}\Delta\phi^{\alpha-1}\right) \tag{28}$$

In the 2D case, the energy release rate $G = G^\mathrm{I} + G^\mathrm{II} + G^\mathrm{IV}$ is calculated from F_1, F_2 and ω (i = 1,2). If a 3D crack configuration is considered, there is an additional term G^III from F_3 and Δu_3. In this case, corresponding node sets have to be considered along the crack front for the calculation of local energy release rates. Δa in Eq. (28) is then replaced by local areas of crack extension ΔA. In the case of a curved crack front, the areas ΔA on the crack faces and on the ligament are different and have to be weighted.[22] The numerical realisation of the MCCI technique for singular quarter point crack tip elements has been elaborated by Kemmer.[21]

3.3. The electromechanical J-integral

The well known J-integral can be extended to electromechanical crack problems and computed by the equivalent domain integral method. Here, it is used to calculate the energy release rate G.

First, we consider a 2D crack problem, i.e. a plane through-thickness crack in a piezoelectric body of arbitrary shape, see Fig. 5. The electromechanical J-integral vector is defined as[23]

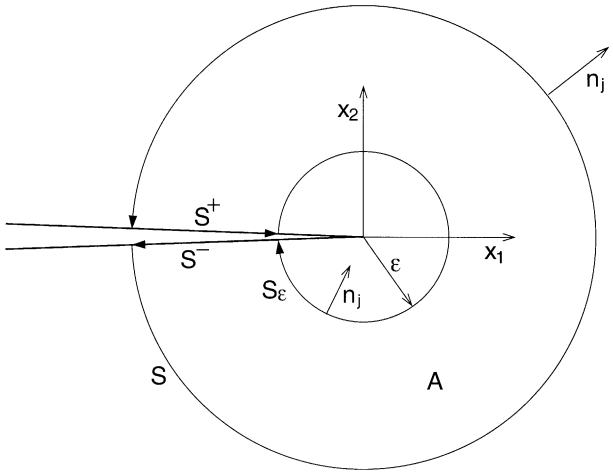

Fig. 5. Integration paths around a crack tip for the illustration of the J-integral.

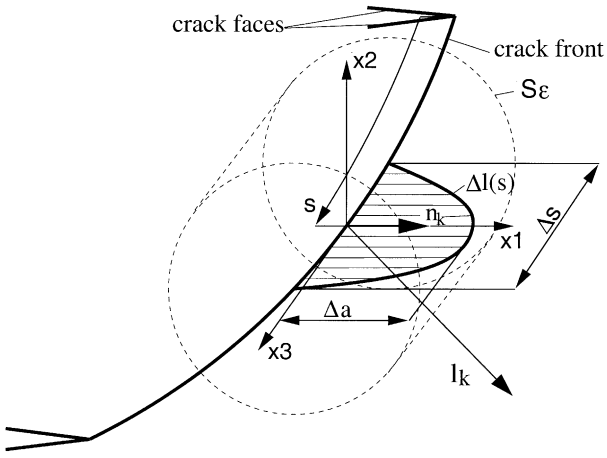

Fig. 6. Illustration of the virtual crack extension technique for the 3D J-integral.

$$J_k = -\lim_{\varepsilon \to 0} \int_{S\varepsilon} \left(H\delta_{kj} - \sigma_{ij}u_{i,k} + D_j E_k\right) n_j ds = -\lim_{\varepsilon \to 0} \int_{S\varepsilon} Q_{kj} n_j ds \tag{29}$$

with the electrical enthalpy density

$$H = \frac{1}{2}\left(\sigma_{ij}\varepsilon_{ij} - D_i E_i\right) \tag{30}$$

In Eq. (29) δ_{kj} is the unit tensor, n_j is the outward normal of the domain A and S_ϵ is the interior boundary around the crack tip of the closed contour $\Gamma = S + S^+ + S_\varepsilon + S^-$. In analogy to elastostatics, the term Q_{kj} is called the generalised energy momentum tensor. For $k=1$, Eq. (29) yields the energy release rate, i.e. $J_1 = G$.

For the sake of a more convenient numerical treatment, Eq. (29) is transformed into an equivalent domain integral. Therefore, a continuously differentiable weighting function[24] q is introduced, being $q=1$ on the boundary S_ϵ and $q=0$ on the outer part of the boundary S. Applying Gauss's integral theorem, the J-integral can be expressed in terms of a domain integral and a contour integral over the crack faces:

$$J_k = \int_A \left(Q_{kj}q\right)_{,j} dA - \int_{S^+ + S^-} Q_{kj} q n_j ds \tag{31}$$

The numerical realisation of the 2D case has been treated in.[25] In the 3D case, we consider a segment Δs of the crack front, surrounded by an inner tube S_ϵ and an outer closed surface S. Now, the weighting function is a vector q_k. To calculate local values of J along the crack front, a vector l_k is introduced, see Fig. 6. It lies in the crack plane and determines an area of virtual crack extension, which is defined by the enveloping curve $\Delta l(s) = \Delta a l_k n_k$. Therefore, this method is called the virtual crack extension technique. q_k is 0 on the outer surface S. On the inner surface S_ϵ, q_k differs from 0 only within a section Δs along the crack front, in which $q_k = l_k$. The mean value $\overline{J}$ within the section Δs is

$$\overline{J} = \int_V Q_{kj} q_{k,j} dV + \int_V \left(H_{,k}|_{\exp} + b_i u_{i,k} + \omega_V E_k\right) q_k dV - \int_{S^+ + S^-} \left(H n_k - T_i u_{i,k} - \omega_S E_k\right) q_k dS \tag{32}$$

where V is the enclosed volume between S_ϵ and S, i.e. the integration domain. The local result along the crack front is calculated from the simplified relation

$$J(s) = \frac{\overline{J}}{\int_{\Delta s} l_k n_k ds} \tag{33}$$

For 3D crack analysis the J-integral is a scalar yielding the energy release rate. The second domain integral in Eq. (32) dispappears, if there are no volume tractions and charges ($b_i, \omega_V = 0$) and if the material properties are homogeneous $\left(H_{,k}|_{\exp} = 0\right)$. The boundary integral disappears if mechanical tractions and electric charges on the crack faces vanish ($T_i, \omega_S = 0$) and if the crack face normals coincide with the unit vector e_{x2} of the crack coordinate system ($n_k q_k = 0$).

4. Fracture experiments with DCB specimens

To investigate the fracture characteristic of ferroelectric ceramics under combined electromechanical loading, experiments with DCB specimens have been carried out and evaluated.[26,27] The most common fracture testing devices for smart ceramic materials are compact tension, three/four point bending and Vickers indentation

specimens.[7,20,28] Here, the displacement controlled DCB experiment has been chosen, since the crack propagation can be kept stable for several millimeters. This enables us to change the loading conditions during the experiment and to observe their effect on the crack growth in situ.

4.1. Preparation of the specimen and experimental set-up

The specimen is made of coarse-grained barium titanate with an average grain size of 20 μm and a 0.5 mol% TiO_2 doping.[29] In Fig. 7 the DCB specimen is illustrated. Its size is 4×4×17 mm. On one of the smaller faces a notch of about 200 μm is sawn into the material with a depth of 3 mm. The ground of the notch is prepared with a razor blade. A radius between 10 and 15 μm is thus accomplished facilitating the crack initiation. To avoid crack kinking, a guiding groove is prepared parallel to the notch along the whole length of the specimen. Its width and depth are 500 μm and 2 mm, respectively.

For the electric loading two thin gold layers are sputtered onto a ground layer of chrome, guaranteeing a uniform electric voltage U along the electrodes, which are aligned parallel to the plane of crack propagation. On the ligament, far enough from the crack tip to have homogeneous fields, the electric field is orientated perpendicular to the crack faces having an intensity $E = U/2h$. The material poling is carried out after the sintering, applying an electric voltage at the electrodes before falling below the Curie temperature. Notch and guiding groove are prepared at the poled material.

The crack initiation is done mechanically, driving a wedge of ZrO_2 into the notch, see Fig. 7. The wedge is moved by a piezoelectric actuator, showing a linear displacement-over-voltage behaviour. Specimen and actuator are fixed within a stiff frame. While the wedge is driven continuously into the notch, the crack opening displacement (COD) δ_l is measured optically with a precision of 0.05 μm. It is most convenient to measure δ_l at the edges of the guiding groove. The crack length a is determined on the face opposite to the guiding groove by a long distance microscope.

4.2. Evaluation of the experimental data

While the COD is a linear function of time, in Fig. 8 the crack length a is plotted vs. the time. In the interval between 66 and 137 s the specimen is additionally loaded by an electric field of 750 V/mm, which is directed into the poling direction $\vec{P}$. Obviously, the electric field slows down the crack growth. When the field is switched off, the crack seeks equilibrium and accelerates until the corresponding crack length is reached. The crack velocity plotted in Fig. 8 has been calculated by numerical differentiation of the crack length. If the electric field on the ligament far from the crack tip is orientated antiparallel to the poling direction, the electric field has the same influence on the crack growth. This can be explained by a repolarisation of the specimen, since the applied electric loads are much above the coercive field of barium titanate. Since repolarisation in ferroelectrics is a transient process, which is well known from relaxation experiments, it takes some seconds after the field has been switched on to obtain reproducable results. The time-dependent character of repolarisation is also responsible for the delay of the decrease and increase of the crack velocity in Fig. 8.

The loading of the crack is uniquely determined by the COD δ_l, the voltage U and the crack length a. In order to transfer the experimental results of the specific DCB-geometry into relevant crack tip parameters, the field intensity factors K_I and K_{IV} are calculated. Both K_I and K_{IV} can be separated into a mechanical part (superscript m), which is due to mechanical loads and an electrical part (superscript e). The total field intensity factors are

$$K_{I,IV} = K^m_{I,IV} + K^e_{I,IV} \tag{34}$$

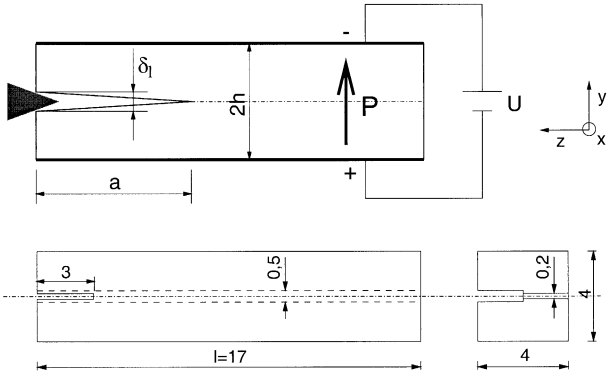

Fig. 7. Geometry and electromechanical loading conditions of the DCB specimen.

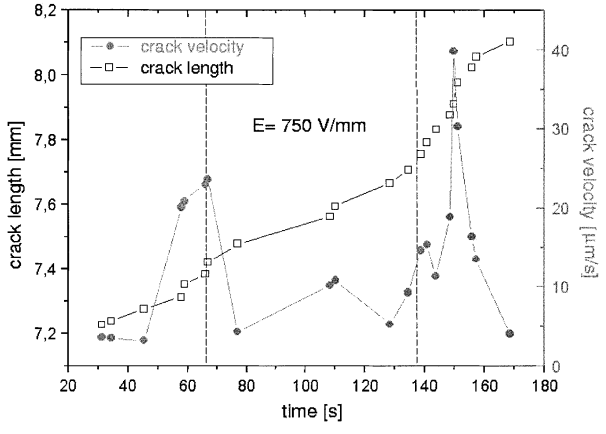

Fig. 8. Crack length and crack velocity vs. time.

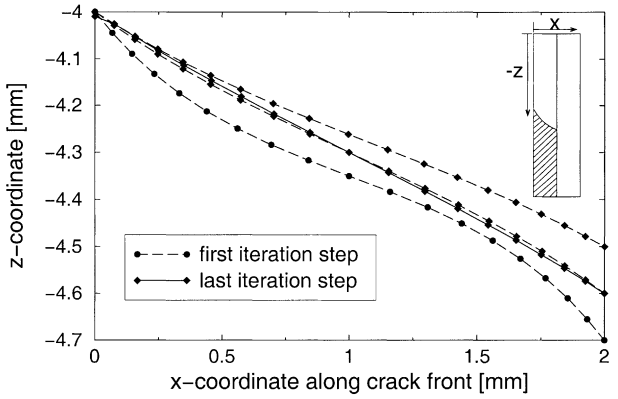

Fig. 9. Shape of a crack front calculated numerically applying an iteration scheme.

A formula for the calculation of K_I^m is suggested in Murakami's handbook.[30] With the notations according to Fig. 7 it is given by

$$K_I^m = \frac{\sqrt{3}E'\delta_l}{4\sqrt{h}\left(\frac{a}{h}+0,64\right)^2} \tag{35}$$

For the plane strain state $E' = E/(1-\nu^2)$ with Young's modulus E and Poisson's ratio ν. Applying Murakami's formula, E and ν have been given average values for an isotropic body, calculated from the elastic constants of the anisotropic material.

Eq. (35) has been derived for a classical DCB specimen with rectangular cross sections of the beams and a plane through-thickness crack. Our specimen is different, because of the guiding groove going along with L-shaped cross sections. Furthermore, the crack front is curved. Therefore the crack length a, depicted in Fig. 7, has to be interpreted as an average crack length along the crack front. A possible deviation of K_I^m calculated from Eq. (35) is investigated applying finite element calculations in connection with the numerical methods presented in Section 3

Fig. 9 shows four hypothetical shapes of crack fronts. The arrangement of the coordinates x and z is depicted in the small sketch. Due to the guiding groove, the ligament (hatched area) ends in the middle of the specimen at $x=2$ mm. The material constants of barium titanate (see Appendix B) have been chosen for the calculation of K_I^m for the different crack front shapes. If a simple fracture criterion $K_I^m = K_{IC} = \text{const}$ is applied, such a shape will prevail, which shows a constant K_I^m along the crack front. Thus, the correct shape of the crack front was found by an iteration procedure, leading to the solid line in Fig. 9. The corresponding stress intensity factor for an exemplary COD of $\delta_l = 4\mu$m is $K_I^m = 0.58$ MPa m$^{1/2}$. For $a=4$ mm, which is the crack length measured on the surface of the specimen according to Fig. 9, Eq. (35) yields $K_I^m = 0.65$ MPa m$^{1/2}$ for the same COD.

To avoid the effort of performing finite element calculations for the evaluation of each DCB experiment, similar iterative calculations are carried out of the kind presented in Fig. 9 for two more crack lengths $a(x=0) = 6/8$ mm. By interpolation of the numerical data a correction formula is introduced, improving the accuracy of Murakami's formula, Eq. (35). The corrected value $K_{I,cor}^m$ for arbitrary crack lengths a within the range 3.5–8.5 mm is calculated using Eq. (35) in connection with

$$\frac{K_{I,cor}^m - K_{I,mur}^m}{K_{I,cor}^m} = -0,714\cdot e^{-a} + 1,4\times 10^{-2}. \tag{36}$$

The relative errrors for the stress intensity factors determined by Murakami's formula $\left(K_{I,mur}^m\right)$ lie between -12% and $+2\%$.

In Fig. 10 the stress intensity factor K_I^m, calculated from the experimental data, is presented. Numerical

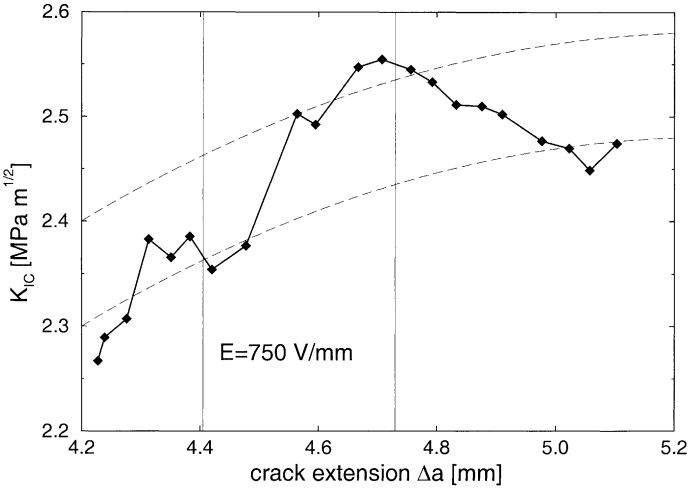

Fig. 10. Fracture toughness K_{IC} calculated from the experimental data.

calculations proved, that K_I^e due to electrical loads can be neglected for the material constants of barium titanate compared with the K_I^m induced by the mechanical load. Therefore, according to Eq. (34) $K_I \approx K_I^m$. Furthermore, due to the stable critical crack growth all calculated fracture quantities (applied loading) equal their critical values (material resistance). For that reason, Fig. 10 shows the fracture toughness K_{IC}, which is plotted vs. the crack extension Δa. The graph shows a rising crack resistance curve (R-curve). Due to the action of the electric field the fracture toughness increases effecting the drop of the crack velocity presented in Fig. 8. When the electric field is switched off, K_{IC} falls down to the original R-curve. Again, time-dependent repolarisation delays the change of the fracture toughness. The dashed lines schematically depict the shifting of the R–curve caused by the superposition of an electric load. The effects described here will be explained by the micromechanical process zone model.

The electric displacement intensity factor K_{IV} has to be calculated numerically, following the iterative procedure outlined for the determination of K_I. In contrast to the stress intensity factor, both mechanical and electrical loads have an essential influence on K_{IV}. In order to prevent the effort of numerical calculations for each set of measured data, dimensionless geometry functions β_{IV}^m and β_{IV}^e are computed relating mechanical and electrical loads, represented by δ_l and U, to the intensity factors K_{IV}^m and K_{IV}^e:

$$K_{IV} = K_{IV}^m + K_{IV}^e = \sqrt{\pi a}\left[\frac{3e_{33}h}{4a^2}\beta_{IV}^m\left(\frac{a}{h}\right)\delta_l + \frac{\kappa_{33}}{2h}\beta_{IV}^e\left(\frac{a}{h}\right)U\right] \tag{37}$$

The piezoelectric and dielectric constants e_{33} and κ_{33}, respectively are included in Appendix B. To determine the geometry functions, numerical calculations for different crack lengths a have been carried out. The results are very well represented by the polynomials

$$\begin{aligned}\beta_{IV}^m &= -8,52\cdot10^{-2} + 3,23\cdot10^{-1}\left(\frac{a}{h}\right) - 1,806\cdot10^{-1}\left(\frac{a}{h}\right)^2 \\ &\quad + 5,025\cdot10^{-2}\left(\frac{a}{h}\right)^3 - 7,02\cdot10^{-3}\left(\frac{a}{h}\right)^4 + 3,9\cdot10^{-4}\left(\frac{a}{h}\right)^5 \\ \beta_{IV}^e &= 1,23 - 0,452\left(\frac{a}{h}\right) + 9,5\cdot10^{-2}\left(\frac{a}{h}\right)^2 \\ &\quad - 7,47\cdot10^{-3}\left(\frac{a}{h}\right)^3\end{aligned} \tag{38}$$

The energy release rate can be separated into a mechanical part G_m, accounting for the change in the elastic energy and an electric part G_e considering the rate of change in the electric energy. For the important case of a perpendicular orientation of the crack faces with respect to the poling axis Eq. (3) yields[15]

$$\begin{aligned}G &= G_m + G_e \\ &= \frac{1}{2}\left(\frac{K_I^2}{c_T} + \frac{K_{II}^2}{c_L} + \frac{K_{III}^2}{c_A} + \frac{K_I K_{IV}}{e}\right) + \frac{1}{2}\left(\frac{K_I K_{IV}}{e} - \frac{K_{IV}^2}{\kappa}\right)\end{aligned} \tag{39}$$

In Fig. 11 the mechanical and the electromechanical energy release rates G_m and G_{em} are plotted, calculated from the experimental data. The corresponding values of K_I and K_{IV} have been converted into the energy release rates by Eq. (39). As the figure shows, G_m is increased due to the electric field. Since G_e has a negative sign, the total energy release rate is decreased.

5. Micromechanical model of the fracture process zone

To calculate the influence of ferroelectric/−elastic domain switching within the fracture process zone on the fracture toughness, a micromechanical model has been developed. First, a switching criterion is applied, localising switching events due to external loads. In a second step

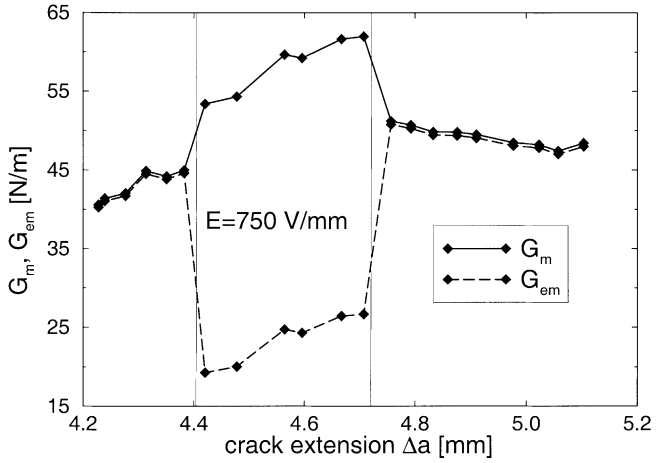

Fig. 11. Mechanical and electromechanical energy release rates G_m and G_{em} vs. Δa.

the spontaneous change of the fracture toughness is calculated, based on the shape of the switching zone.

5.1. Shape of the fracture process zone

The load induced stress and electric displacement fields within the cracked body give rise to the switching of domains. It is assumed that the switching is restricted to small regions around the crack tips (small scale switching), which will be called the process zones. This assumption holds, if switching is only caused by the inhomogeneous fields concentrated around a crack tip, whereas homogeneous fields in the absence of cracks do not change the direction of polarisation. This is usually the case with technical actuators, since the loading directions are not changed during service conditions. The state of polarisation is fixed after poling and will only be changed locally due to cracks.

The domain switching model applied here is a very simple one. Details[9,10] like domain wall motion, twinning or the arrangement of domains, as well as grain boundaries are neglected. We consider unit cells of a tetragonal crystal lattice which are allowed to change the local states of polarisation and strain in the material by switching independently from neighbouring cells. Furthermore, the model is restricted to switches in the crack plane, therefore three variants have to be taken into account. The c-axes of a cell can rotate 90° clockwise(–) or counterclockwise(+) as well as 180°. A simple switching criterion[31] is applied to determine whether switching occurs:

$$\sigma_{ij}\Delta\varepsilon_{ij} + E_i\Delta P_i \geqslant 2E_C P^0 \tag{40}$$

The threshold value on the right hand side of Eq. (40) approximately represents half of the area of a polarisation hysteresis with the coercive field E_C and the remanent polarisation P^0. Assuming that stresses σ_{ij} and electric fields E_i remain unchanged during switching, the left hand side of Eq. (40) represents the specific switching work, taking into account the spontaneous changes of strain

$$\begin{aligned}\Delta\varepsilon_{ij} &= \varepsilon_D \mathbf{T}(\phi)\begin{pmatrix} -1 & 0 \\ 0 & 1 \end{pmatrix}\mathbf{T}(\phi)^T \\ &= -\varepsilon_D \begin{pmatrix} \cos 2\phi & \sin 2\phi \\ \sin 2\phi & -\cos 2\phi \end{pmatrix}\end{aligned} \tag{41}$$

and polarisation

$$\Delta P_i = bP^0 \begin{pmatrix} \sin(\phi+\varphi) \\ -\cos(\phi+\varphi) \end{pmatrix} \tag{42}$$

$$b = \begin{cases} -\sqrt{2} \text{ for } +90^\circ \\ \sqrt{2} \text{ for } -90^\circ \\ -2 \text{ for } \pm 180^\circ \end{cases}, \varphi = \begin{cases} +\pi/4 \text{ for } +90^\circ \\ -\pi/4 \text{ for } -90^\circ \\ +\pi/2 \text{ for } \pm 180^\circ \end{cases}$$

In Eq. (41) the strain tensor is transformed from a local lattice coordinate system to the global crack coordinate system (x_1, x_2), see Fig. 1, by means of the transformation matrix $\mathbf{T}(\phi)$. ϕ is the angle between the c-axes and x_1, $\varepsilon_D = (c-a)/a_0$ contains the lattice papameters of the tetragonal and cubic phases. The induced strains are equal for $+90^\circ$ and -90° switching and vanish for a switch of 180°, whereas the change of polarisation ΔP_i differs for the three variants.

The switching criterion Eq. (40) is used to decide, if domain switching occurs at arbitrary locations in the crack plane. If there are several possibilities, i.e. $\pm 90^\circ$ and 180° switching events, the one will prevail which goes along with the maximum of irreversible switching work. For the calculation of the switching work, results from the closed-form solution of the Griffith crack are used. Stresses σ_{ij} are inserted from Eq. (9), the electric field $E_i = -\phi_{,i}$ can be calculated inverting the constitutive equations, Eq. (7). Using the analytical solutions, local changes of the elastic anisotropy and the direction of polarisation due to switching do not interact with the fields σ_{ij} and E_i. Therefore the results are first order approximations.

Since 180° events do not change the state of strain, only $\pm 90^\circ$ events are considered for the fracture process zone. Fig. 12 shows three process zones around one crack tip of a Griffith crack (see Fig. 1) for a constant mechanical Mode-I load $\sigma_{22}^\infty = 150$ MPa and different electric loads. If a crack length $a = 10^{-4}$ m is chosen, a stress intensity factor is obtained, which coincides with typical fracture toughnesses of piezoelectric ceramics by order of magnitude. In accordance with the experimental conditions the poling axis was chosen perpendicular to the crack faces. Following Eq. (12) the electric loading is realised by the remote electric displacement D_2^∞. E_2^∞ is calculated from the inverse constitutive Eq.

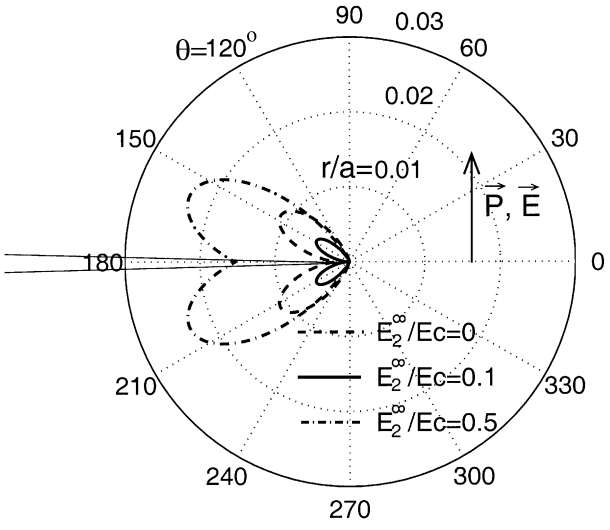

Fig. 12. Fracture process zones for a mechanical Mode-I crack opening and different electric loads.

(7). E_1^∞ disappears for the given loading $\left(\sigma_{22}^\infty, D_2^\infty\right)$ and poling conditions, therefore the remote electric field is aligned perpendicular to the crack faces. Furthermore, the crack is assumed impermeable with respect to electric fields, i.e. $D_2^C = 0$.

In Fig. 12 the radial coordinate r is normalised with respect to the half crack length a. Considering the extension of the three process zones, it has to be noticed that there is a minimum for an electrical load between 10% and 20% of the coercive field E_C. The decreasing size of the fracture process zone for low field intensities is conditioned by the compensation of the initial electric field due to the piezoelectric effect.

5.2. Influence of domain switching on the fracture toughness

The spontaneous strain $\Delta\varepsilon_{ij}$ [Eq. (41)] is homogeneous within the fracture process zone, depending on the direction of polarisation ϕ, and vanishes outside. Because of this strain discontinuity spontaneous tractions $\bar{t}_i$ are induced at the boundary of the process zone, which can be interpreted as residual stresses. If the crack grows by Δa, see Fig. 13, the homogeneous switching zone will be extended along the crack faces. In Fig. 13 the boundary of the original process zone is represented schematically by the solid lines, the dashed lines depict the extension of the switching zone for $\Delta a > 0$. Thus, the width of the wake w is determined by the lateral extension of the process zone, Fig. 12. The assumption of a homogeneous strain $\Delta\varepsilon_{ij}$ within the extended switching zone requires the switched domains not to be exposed to further switches when the crack grows.

The influence of point loads F_i on the field intensity factors is expressed by the weight functions h_{iL} [Eqs. (19),(20)]. The field intensity factors ΔK_L due to the tractions $\bar{t}_i$ are calculated by integrating along the boundary S of the switching zone, see Fig. 13:

$$\Delta K_L = \oint_S \bar{t}_i h_{iL} ds \tag{43}$$

Eq. (43) has been used for the modelling of transformation toughening by McMeeking and Evans.[32] Yang and Zhu applied the weight function method to the calculation of switch-toughening assuming uniform electric fields[33] and non-uniform fields[34] neglecting both elastic and dielectric anisotropy as well as electromechanical field coupling.

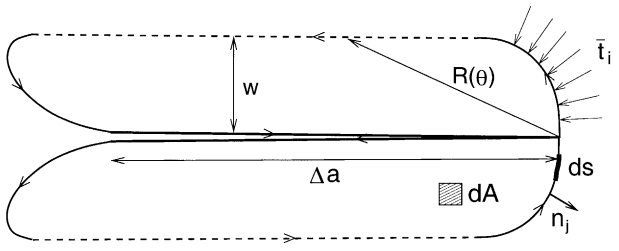

Fig. 13. Switching zone and integration contour around a crack grown by the amount Δa.

The vector of tractions $\bar{t}_i$ can be expressed in terms of the stress tensor $\bar{\sigma}_{ik}$ and the outward normal n_k. Applying Gauss's integral theorem and accounting for the fact that $\bar{\sigma}_{ik}$ is constant, the line integral in Eq. (43) can be transformed into a domain integral

$$\Delta K_L = \int_A (\bar{\sigma}_{ik} h_{iL})_{,k} dA = \int_A \bar{\sigma}_{ik} h_{iL,k} dA \tag{44}$$

The total field intensity factors K_L^{tip} are gained from a superposition of ΔK_L and the contributions due to remote loads K_L^∞.

A fracture criterion according to Eq. (4) has to be determined next. It is assumed, that only mechanical stresses are relevant on the left hand side of the criterion, whereas the influence of electric fields is taken into account in terms of ΔK_L on the right hand side of the equation. Restricting mechanical loads to the case of a pure Mode-I crack opening, the fracture criterion is assumed to be

$$K_{\mathrm{I}}^{tip} = K_{\mathrm{IC}}^{tip} = K_{\mathrm{I}}^\infty + \Delta K_{\mathrm{I}} \tag{45}$$

The intrinsic fracture toughness K_{IC}^{tip} is a material inherent parameter for brittle cleavage fracture. ΔK_{I} supplies an additional loading or unloading of the crack tip due to domain switching processes. According to Eq. (45) it reduces or enhances K_{I}^∞ and thus the fracture load. Therefore it can also be interpreted as a microstructural contribution to the fracture toughness yielding a fracture criterion

$$K_{\mathrm{I}}^\infty = K_{\mathrm{IC}}^{tip} - \Delta K_{\mathrm{I}} = K_{\mathrm{IC}}^\infty\left(\Delta a, \phi, K_{\mathrm{I}}^\infty, K_{\mathrm{IV}}^\infty\right) \tag{46}$$

The symbols in parentheses indicate that the effective fracture toughness K_{IC}^∞ depends on mechanical and electrical crack tip fields as well as on crack growth (R-curve) and the poling direction. In general, the left hand side of the fracture criterion Eq. (46) is determined from analytical or numerical calculations of stress intensity factors accounting for piezoelectric material behaviour.

For the calculation of ΔK_{I} according to Eq. (44), the weight function for mode $L \equiv \mathrm{I}$ h_i^{I} is required. It will be taken from Eq. (24), neglecting the deviation of the results for isotropic and piezoelectric material behaviour (see Fig. 3). Since for barium titanate the material anisotropy seems to be of minor significance, the stress tensor $\bar{\sigma}_{ij}$ is expressed in terms of the spontaneous strain $\Delta\varepsilon_{ij}$ [(Eq. (41)] using Hooke's law of isotropic elasticity:

$$\bar{\sigma}_{ij} = \frac{E}{1+\upsilon}\left(\Delta\varepsilon_{ij} + \frac{\upsilon}{1-2\upsilon}\Delta\varepsilon_{ll}\delta_{ij}\right) = \frac{E}{1+\upsilon}\Delta\varepsilon_{ij} \tag{47}$$

with Young's modulus E and Poison's ratio ν. It was taken into account, that the trace of the strain tensor $\Delta\varepsilon_{ll}$ vanishes. Inserting Eq. (47) into Eq. (44) yields

$$\Delta K_{\mathrm{I}} = \frac{E}{1+\upsilon}\int_A \Delta\varepsilon_{ij} h^I_{i,j}\, dA \tag{48}$$

The effective fracture toughness K^{∞}_{IC} is calculated from Eq. (46) inserting Eqs. (41) and (24) into Eq. (48) and integrating in polar coordinates:

$$K^{\infty}_{\mathrm{IC}} = K^{tip}_{\mathrm{IC}} + \frac{3\varepsilon_D E}{4\sqrt{2\pi}(1-\upsilon^2)} \times \int_{-\pi}^{\pi} \sqrt{R(\theta)}\left[\cos\left(2\phi - \frac{7\theta}{2}\right) - \cos\left(2\phi - \frac{3\theta}{2}\right)\right] d\theta \tag{49}$$

$R(\theta)$ denotes the radial coordinate of the switching zone boundary, see Fig. 13. The integration over θ is performed numerically, since $R(\theta)$ is not available in closed form.

In Fig. 14 the effective fracture toughness K^{∞}_{IC} according to Eq. (49) is plotted vs. the crack growth Δa, which has been normalised with respect to the height of the switching zone w (see Fig. 13). The calculations are based on the material data of barium titanate, see Appendix B. To estimate the influence of the microstructure on the fracture toughness, particularly in connection with electric loading, the Griffith crack according to Fig. 1 is exposed to a mechanical load σ^{∞}_{22} and electrical loads of three different intensities. The corresponding fracture process zones are those shown in Fig. 12. They supply the function $R(\theta)$ which is inserted into Eq. (49). The intrinsic fracture toughness $K^{tip}_{\mathrm{IC}} = 2,65$ MPa $\mathrm{m}^{1/2}$ is chosen arbitrarily yielding results representing the typical range of the fracture toughness of ferroelectric ceramics. K^{tip}_{IC} is depicted in Fig. 14 by the solid straight line.

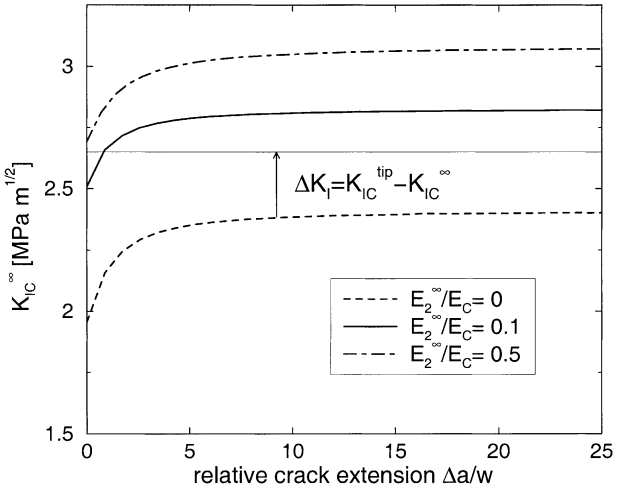

Fig. 14. Crack resistance curves (R-curves) for a mechanical Mode-I crack opening and different electric loads. Poling and electric load perpendicular to the crack faces.

Fig. 14 shows a typical R-curve behaviour. The fracture toughness enhances with an increasing crack length reaching a plateau value for $\Delta a \approx 20\ w$. In the case of a pure mechanical loading ΔK_{I} has a positive sign, i.e. the effective fracture toughness is reduced. On the other hand, K^{∞}_{IC} increases if an electric field is superimposed. In this case, the fracture process zone effects a shielding of the crack tip. In Fig. 14 the maximum electric load E^{∞}_2 is 50% of the coercive field. The corresponding increase of the fracture toughness is about 25%, which has to be considered as an upper bound for the given E^{∞}_2. If the electrical permeability of the crack were taken into account, the effect would be reduced according to Eq. (12).

6. Summary and conclusions

Fracture experiments with DCB specimens made of barium titanate have been evaluated to investigate the influence of electric fields on the fracture toughness of ferroelectric/elastic ceramics. During a stable crack growth for several millimeters, R-curves could be calculated from the measured data: crack opening displacement, crack length and electric potential. Moreover, it was possible to observe the influence of electric fields on the crack growth in situ. To evaluate the measured data, numerical methods have been developed, allowing for the calculation of the J-integral, the energy release rate and the field intensity factors for piezoelectric materials. The numerical tools can also be applied to the fracture mechanical analysis of arbitrary cracked bodies under electromechanical loading.

A generalisation of the classical analytical fracture mechanics towards piezoelectric materials is presented for the Griffith crack problem. It gives principal insight into electrical and mechanical fields around a crack tip and into effects of piezoelectric field coupling. Energy release rates and field intensity factors are calculated and their relation is derived in terms of the Irwin matrix. Weight functions are derived allowing for the calculation of mechanical and electrical intensity factors for arbitrary loading conditions. This analytical foundation is essential for the develpoment of numerical methods and is the basis of the process zone model.

To evaluate the strength of piezoelectric structures, a fracture criterion is introduced relating stress intensity factors, gained from numerical or analytical analyses, to a fracture toughness. The electric intensity factor K_{IV} is excluded from the fracture criterion. Nevertheless, the numerical stress analysis accounts for the influence of an electric field on the mechanical stress intensity factors. The essential effect of electric loads is included in the fracture toughness, yet. Domain switching is

responsible for a shielding effect, which makes the fracture toughness a function of loads, the crack growth Δa and the poling direction.

To investigate the influence of loads on the fracture toughness, a micromechanical model of the fracture process zone has been developed. It is based on an analytical solution of the piezoelectric Griffith crack problem and uses a simple ferroelectric/elastic domain switching criterion. It neglects the interaction of switching in the process zone and the driving electrical and mechanical fields. Therefore, it has to be considered as a first order approximation. R-curves have been predicted calculating the influence of electric loads on the fracture toughness and quantifying the material side of the fracture criterion.

To compare the calculated results with those from the fracture experiments, the poling direction and the remote electric field have been chosen perpendicular to the crack faces. Since the crack tip fields are not influenced by the geometric boundary conditions, results from the Griffith crack and a cracked DCB specimen can be compared. Figs. 14 and 10 show, that the micromechanical model is able to predict the principal influence of an electric field, leading to an increase of the fracture toughness for the given configuration. A quantitative comparison of the results is only possible, if the electrical permeability of the crack is taken into account.

Acknowledgements

The German Research Foundation (DFG) is gratefully acknowledged for financial support within the research program "Multifunktionswerkstoffe"

Appendix A. Derivation of piezoelectric weight functions

Fracture mechanics weight functions have been derived by Bückner[35] and Rice[36] for an isotropic, elastic material. Here, weight functions for anisotropic piezoelectric materials will be presented, which have recently been derived by McMeeking and Ricoeur.[37] We consider a Griffith crack under two loading conditions, see Fig. 1. On the one hand remote uniform loads $T_N = \sigma_{i2}^{\infty}$ and D_2^{∞} are applied (subproblem 1), on the other hand point forces and charges $F_N = \left(F_i, Q\right)^T$ are acting at $x_i = r(\cos\theta, \sin\theta)^T$ (subproblem 2). Finite electrical permeability of the crack is neglected in the following, although the theory is valid for arbitrary loads on the crack faces. Due to linear superposition the field intensity factors are [see Eq. (14)]

$$K_M = \sqrt{\pi a} T_M + h_{MN} F_N \tag{50}$$

In Eq. (50) the weight functions h_{MN} have been introduced, allowing for the calculation of K-factors due to point loads. Remote displacements/potentials u_M^{∞} and displacements/potentials at x_i due to applied loads T_N and F_N can be expressed in terms of

$$\begin{aligned} u_M^{\infty} &= C_{MN}^{1} T_N + C_{MN}^{12} F_N(x_i) \\ u_M(x_i) &= C_{MN}^{21} T_N + C_{MN}^{2} F_N(x_i) \end{aligned} \tag{51}$$

whereby C_{MN}^{1} and C_{MN}^{2} are the compliances of the subproblems 1 and 2, respectively. $C_{MN}^{12} = C_{MN}^{21}$ are the cross compliances of both subproblems, which are identical according to Betti's theorem of reciprocity. The total potential energy Π for the superposition of both load cases can be introduced as the difference of the internal energy U of the cracked body and the external loads:

$$\Pi(T_N, F_N, a) = U - T_N u_N^{\infty} - F_N(x_i) u_N(x_i) \tag{52}$$

Accounting for Eq. (51), the total potential energy is a function of the loads T_N, F_N and the crack length $l = 2a$. A Legendre transformation between the variables Π and U shows, that Eq. (52) is valid only, if the partial derivatives

$$\begin{aligned} u_N(x_i) &= -\frac{\partial \Pi(T_N, F_N, a)}{\partial F_N}; \\ u_N^{\infty} &= -\frac{\partial \Pi(T_N, F_N, a)}{\partial T_N} \end{aligned} \tag{53}$$

exist. The energy release rate was defined in Eq. (2). Taking into account that there are two crack tips, the energy release rate is

$$G = -\frac{1}{2}\frac{\partial \Pi(T_N, F_N, a)}{\partial a} \tag{54}$$

Differentiating Eq. (54) with respect to F_N and inserting Eq. (53) yields

$$\frac{\partial G}{\partial F_N} = -\frac{1}{2}\frac{\partial^2 \Pi(T_N, F_N, a)}{\partial a \partial F_N} = \frac{1}{2}\frac{\partial U_N(x_i)}{\partial a} \tag{55}$$

On the other hand the energy release rate can be related to field intensity factors according to Eq. (3). Furthermore, taking into account Eq. (50) leads to

$$G = \frac{1}{2}\left(\sqrt{\pi a} T_M + h_{MN} F_N\right) Y_{MK} \left(\sqrt{\pi a} T_K + h_{KL} F_L\right) \tag{56}$$

Differentiating Eq. (56) with respect to F_N as well as $u_M(x_i)$ in Eq. (51) with respect to the half crack length a and subsequently inserting both equations into Eq. (55) yields

$$2\left(\sqrt{\pi a}T_N + h_{NK}F_K\right)Y_{NL}h_{LM} = \frac{dC^{12}_{MN}}{da}T_N + \frac{dC^{2}_{MN}}{da}F_N(x_i) \tag{57}$$

The goal is to calculate weight functions h_{LM} from known solutions of the subproblem 1. Therefore, the point loads F_N in Eq. (57) will be chosen zero, which is possible since weight functions are a property of the geometry of the boundary value problem and do not depend on loading conditions. For $F_N = 0$ Eq. (57) yields

$$h_{LN} = \frac{1}{2\sqrt{\pi a}}Y^{-1}_{LM}\frac{dC^{12}_{MN}}{da} \tag{58}$$

According to Eq. (51) the compliances C^{12}_{MN} are equal to the displacements and potentials u_M at x_i due to unit stresses and electric displacements T_N at infinity. In connection with Eq. (11) it is obvious that

$$C^{12}_{MN} = \Re\left\{A_{M\alpha}N_{\alpha N}\left[\left(z^2_\alpha - a^2\right)^{\frac{1}{2}} - z_\alpha\right]\right\} \tag{59}$$

The term which is linear in z_α can be omitted, since it describes a homogeneous field which is not influenced by the crack. The derivation with respect to a has to be performed in a crack tip coordinate system accounting for the transformation $\hat{x}_1 = x_1 + a$. Inserting Eq. (59) into Eq. (58) finally gives the piezoelectric weight functions Eq. (19).

Appendix B. Material constants of $BaTiO_3$

The constitutive relations for barium titanate with the positive x_2-axis as poling axis can be written in contracted notations for the global coordinate system. The indices of the material constants $\overline{c}_{ij}, \overline{e}_{ij}, \overline{\kappa}_{ij}$ are notated with respect to the material axes $\overline{x}_i$, whereby $\overline{x}_3$ corresponds to the poling axis.

$$\begin{pmatrix}\sigma_{11}\\ \sigma_{22}\\ \sigma_{33}\\ \sigma_{23}\\ \sigma_{31}\\ \sigma_{12}\end{pmatrix} = \begin{pmatrix} \overline{c}_{11} & \overline{c}_{13} & \overline{c}_{12} & 0 & 0 & 0\\ \overline{c}_{13} & \overline{c}_{33} & \overline{c}_{13} & 0 & 0 & 0\\ \overline{c}_{12} & \overline{c}_{13} & \overline{c}_{11} & 0 & 0 & 0\\ 0 & 0 & 0 & \overline{c}_{44} & 0 & 0\\ 0 & 0 & 0 & 0 & \frac{\overline{c}_{11}-\overline{c}_{12}}{2} & 0\\ 0 & 0 & 0 & 0 & 0 & \overline{c}_{44}\end{pmatrix} \times \begin{pmatrix}u_{1,1}\\ u_{2,2}\\ u_{3,3}\\ u_{2,3}\\ u_{3,1}\\ u_{1,2}\end{pmatrix} + \begin{pmatrix} 0 & \overline{e}_{31} & 0\\ 0 & \overline{e}_{33} & 0\\ 0 & \overline{e}_{31} & 0\\ 0 & 0 & \overline{e}_{15}\\ 0 & 0 & 0\\ \overline{e}_{15} & 0 & 0\end{pmatrix}\begin{pmatrix}\phi_{,1}\\ \phi_{,2}\\ \phi_{,3}\end{pmatrix}$$

$$\begin{pmatrix}D_1\\ D_2\\ D_3\end{pmatrix} = \begin{pmatrix} 0 & 0 & 0 & 0 & 0 & \overline{e}_{15}\\ \overline{e}_{31} & \overline{e}_{33} & \overline{e}_{31} & 0 & 0 & 0\\ 0 & 0 & 0 & \overline{e}_{15} & 0 & 0\end{pmatrix}\begin{pmatrix}u_{1,1}\\ u_{2,2}\\ u_{3,3}\\ u_{2,3}\\ u_{3,1}\\ u_{1,2}\end{pmatrix} - \begin{pmatrix}\overline{\kappa}_{11} & 0 & 0\\ 0 & \overline{\kappa}_{33} & 0\\ 0 & 0 & \overline{\kappa}_{11}\end{pmatrix}\begin{pmatrix}\phi_{,1}\\ \phi_{,2}\\ \phi_{,3}\end{pmatrix}$$

with the elastic constants [N/m^2]:

$$\overline{c}_{11} = 16.6\times10^{10},\quad \overline{c}_{12} = 7.66\times10^{10},\quad \overline{c}_{13} = 7.75\times10^{10}$$
$$\overline{c}_{33} = 16.2\times10^{10},\quad \overline{c}_{44} = 4.29\times10^{10}$$

the piezoelectric constants [C/m^2]:

$$\overline{e}_{15} = 11.6,\quad \overline{e}_{31} = -4.4,\quad \overline{e}_{33} = 18.6$$

and the dielectric constants [C/(Vm)]:

$$\overline{\kappa}_{11} = 14.343\times10^{-9},\quad \overline{\kappa}_{33} = 16.823\times10^{-9}$$

The relationships between the contracted and expanded notations are given as

$$\overline{C}_{1111} = \overline{C}_{2222} = \overline{c}_{11};\quad \overline{C}_{3333} = \overline{c}_{33};\quad \overline{C}_{1122} = \overline{c}_{12};$$
$$\overline{C}_{1133} = \overline{C}_{2233} = \overline{c}_{13};\quad \overline{C}_{2323} = \overline{C}_{3131} = \overline{c}_{44}$$

$$\overline{C}_{1212} = \frac{\overline{c}_{11}-\overline{c}_{12}}{2};\quad \overline{e}_{311} = \overline{e}_{322} = \overline{e}_{31};\quad \overline{e}_{333} = \overline{e}_{33};$$

$$\overline{e}_{113} = \overline{e}_{323} = \overline{e}_{15}$$

Other orientations of the poling axis can be realized applying a transformation of coordinates.

Coercive field intensity: 200 V/mm
Remanent polarisation: 0.25 N/(Vm)

average elastic constants:

$$E = 1.05\times10^5\text{MPa},\quad \upsilon = 0.315$$

constants of the Irwin matrix:

$$Y_{MN} = \begin{pmatrix}1/c_L & 0 & 0 & 0\\ 0 & 1/c_T & 0 & 1/e\\ 0 & 0 & 1/c_A & 0\\ 0 & 1/e & 0 & -1/\kappa\end{pmatrix}$$

$c_L = 68.42$, $c_T = 72.24$, $c_A = 44.75$ GPa; $e = 112.57$ C/m^2, $\kappa = 18.8\cdot10^{-9}$ C/(V m).

References

1. Anderson, T. L., *Fracture Mechanics*. CRC Press: Boca Raton, Ann Arbor, London, Tokyo, 1995.
2. Gross, D., *Bruchmechanik*. Springer Verlag, Berlin Heidelberg, 1996.
3. Zhang, T.-Y., Zhao, M. and Tong, P., Fracture of piezoelectric ceramics. *Advances in Applied Mechanics*, 2002, **38**, 147–289.
4. Qin, Q.-H., *Fracture Mechanics of Piezoelectric Materials*. WIT Press, Southampton, Boston, 2001.
5. Suo, Z., Kuo, C.-M., Barnett, D. M. and Willis, J. R., Fracture mechanics for piezoelectric ceramics. *J. Mech. Phys. Solids*, 1992, **40**(4), 739–765.
6. Pak, Y. E., Linear electro-elastic fracture mechanics of piezoelectric materials. *International Journal of Fracture*, 1992, **54**, 79–100.
7. Mehta, K. and Virkar, A. V., Fracture mechanisms in ferroelectric–ferroelastic lead zirconate titanate (Zr:Ti = 0.54:0.46) ceramics. *J. Am. Ceram. Soc.*, 1990, **73**(3), 567–574.
8. dos Santos e Lucato, S. L., Lupascu, D. C. and Rödel, J., Effect of poling direction on R-curve behavior in PZT. *J. Am. Ceram. Soc.*, 2000, **83**(2), 424–426.
9. Arlt, G., Review: twinning in ferroelectric and ferroelastic ceramics: stress relief. *Journal of Materials Science*, 1990, **25**, 2655–2666.
10. Arlt, G. and Sasko, P., Domain configuration and equilibrium size of domains in $BaTiO_3$ ceramics. *J. Appl. Phys.*, 1980, **51**(9), 4956–4960.
11. Park, S. B. and Sun, C. T., Effect of electric field on fracture of piezoelectric ceramics. *International Journal of Fracture*, 1995, **70**, 203–216.
12. Pohanka, R. C. and Smith, P. L., *Electronic Ceramics*. Marcel Dekker, New York, 1988.
13. Kuna, M. and Ricoeur, A., Simulation of domain switch-toughening in ferroelectric ceramics. In *Proceedings of the ICF10(CD ROM)*, ed. K. Ravi-Chadar *et al*. Pergamon Press, Honululu, 2001.
14. Erdogan, F., On the stress distribution on plates with collinear cuts under arbitrary loads. In *Proc. of the 4th National Congress of Applied Mechanics*, 1962, pp. 547.
15. Kuna, M., Finite element analyses of crack problems in piezoelectric structures. *Computational Materials Science*, 1998, **13**, 67–80.
16. Abendroth, M., Groh, U., Kuna, M. and Ricoeur, A., Finite element-computation of the electromechanical J-Integral for 2-D and 3-D crack analysis. *International Journal of Fracture*, 2002, **114**, 359–378.
17. Barsoum, R. S., On the use of isoparametric finite elements in linear fracture mechanics. *J. Numer. Methods Engng*, 1976, **10**, 25–37.
18. Kuna, M., FEM–Techniken zur Analyse von Rissen unter elektrischen und mechanischen Beanspruchungen. In *Berichte 26, DVM–Arbeitskreis Bruchmechanik*, Stuttgart, 1997, pp. 369–379.
19. Buchholz, F. G., Improved formulae for the finite element calculation of the strain energy release rate by the modified crack closure integral method. In *Accuracy, Reliability and Training in FEM Technology*, ed. J. Robinson. Dorset, 1984, pp. 650–659.
20. Park, S. B. and Sun, C. T., Fracture criteria for piezoelectric ceramics. *J. Am. Ceram. Soc.*, 1995, **78**, 1475–1480.
21. Kemmer, G., *Berechnung von elektromechanischen Intensitätsparametern bei Rissen in Piezokeramiken*. PhD Thesis, Technical University of Dresden, VDI Verlag, 2000.
22. Shang, F., Kuna, M. and Abendroth, M., Finite element analyses of three-dimensional crack problems in piezoelectric structures. *Engineering Fracture Mechanics* (in preparation).
23. Pak, Y. E., Crack extention force in a piezoelectric material. *J. Appl. Mech.*, 1990, **57**, 647–653.
24. Shih, C.-F., Moran, B. and Nakamura, T., Energy release rate along a three-dimensional crack front in a thermally stressed body. *International Journal of Fracture*, 1986, **30**, 79–102.
25. Kuna, M., Energiebilanzintegrale für Risse in piezoelektrischen Werkstoffen unter elektrischen und mechanischen Beanspruchungen. *Technische Mechanik*, 1995, **15**, 195–204.
26. Ricoeur, A., Kuna, M., Förderreuther, A. and Thurn, G., Konzeption und Interpretation elektromechanischer DCB und CT Versuche an Funktionskeramiken. In *31. DVM Tagung AK Bruchvorgänge*, Darmstadt, 1999, pp. 339–348.
27. Kuna, M. & Ricoeur, A., Theoretical investigations on the cracking of ferroelectric ceramics. In *Proceedings of SPIE: Smart Structures and Materials 2000*, ed. C. S. Lynch, New Port Beach (CA), 2000, pp. 185–196.
28. Wang, H. and Singh, R. N., Crack propagation in piezoelectric ceramics: effects of applied electric fields. *J. Appl. Phys.*, 1997, **81**(11), 7471–7479.
29. Förderreuther, A., *Mechanische Eigenschaften von $BaTiO_3$-Keramiken unter mechanischer und elektrischer Belastung*. PhD Thesis, University of Stuttgart, 2000.
30. Murakami, Y., *Stress Intensity Factors Handbook*, Pergamon Press, 1987.
31. Hwang, S. C., Lynch, C. S. and McMeeking, R. M., Ferroelectric/ferroelastic interactions and polarization switch model. *Acta Metall. Mater.*, 1995, **43**, 2073–2084.
32. McMeeking, R. M. and Evans, A. G., Mechanics of transformation-toughening in brittle materials. *J. Am. Ceram. Soc.*, 1982, **65**(5), 242–246.
33. Yang, W. and Zhu, T., Switch-toughening of ferroelectrics subjected to electric fields. *J. Mech. Phys. Solids*, 1998, **46**(2), 291–311.
34. Zhu, T. and Yang, W., Toughness variation of ferroelectrics by polarization switch under non-uniform electric field. *Acta Mater.*, 1997, **45**(11), 4695–4702.
35. Bückner, H. F., A novel principle for the computation of stress intensity factors. *Z. Angew. Math. Mech.*, 1970, **50**, 529–533.
36. Rice, J. R., Some remarks on elastic crack-tip stress fields. *Int. J. Solids Structures*, 1972, **8**, 751–758.
37. McMeeking, R. and Ricoeur, A., The weight function for cracks in piezoelectrics. *Int. J. Solids Structures* (submitted for publication).